Korean J. Chem. Eng., **28**(11), 2137-2141 (2011)
DOI: 10.1007/s11814-011-0119-0

Scanning tunneling microscopy and tunneling spectroscopy studies of niobium-containing $H_{6+x}P_2W_{18-x}Nb_xO_{62}$ (x=0, 1, 2, 3) Wells-Dawson heteropolyacid catalysts to probe their redox property and oxidation catalysis

Jung Ho Choi, Dong Ryul Park, Sunyoung Park, and In Kyu Song†

School of Chemical and Biological Engineering, Institute of Chemical Processes,
Seoul National University, Shinlim-dong, Gwanak-gu, Seoul 151-744, Korea
(*Received 1 March 2011 • accepted 3 May 2011*)

Abstract−Niobium-containing $H_{6+x}P_2W_{18-x}Nb_xO_{62}$ (x=0, 1, 2, 3) Wells-Dawson heteropolyacids (HPAs) were investigated by scanning tunneling microscopy (STM) and tunneling spectroscopy (TS) in order to elucidate their redox properties. The HPAs formed two-dimensional well-ordered monolayer arrays on graphite surface and exhibited a distinctive current-voltage behavior called negative differential resistance (NDR) in their tunneling spectra. NDR peak voltage measured on HPA molecule was correlated with reduction potential and absorption edge energy determined by electrochemical method and UV-visible spectroscopy, respectively. NDR peak voltage of $H_{6+x}P_2W_{18-x}Nb_xO_{62}$ Wells-Dawson HPAs appeared at less negative voltage with increasing reduction potential and with decreasing absorption edge energy. Oxidative dehydrogenation of isobutyraldehyde was also carried out as a model reaction to probe oxidation catalysis of the HPAs. The trend of NDR peak voltage of $H_{6+x}P_2W_{18-x}Nb_xO_{62}$ Wells-Dawson HPAs was well consistent with the trend of yield for methacrolein.

Key words: Heteropolyacid, Niobium, Scanning Tunneling Microscopy, Negative Differential Resistance, Redox Property

INTRODUCTION

Scanning tunneling microscopy (STM) has demonstrated powerful ability to characterize the surface of conductive materials with atomic-scale resolution [1]. With advances in STM instruments and experimental techniques, however, even non-conductive materials such as aniline [2], terephthalic acid [3], pyridine [4], and Langmuir-Blodgett film [5] have been successfully investigated by depositing them on conductive materials such as gold and graphite. Because STM can provide fundamental microscopic insight with atomic level, some previous researches attempted to elucidate the heterogeneous catalytic system by STM study of a model catalyst system [6,7]. STM can be utilized as a versatile technique for exploring not only structural details but also electronic state of the surface molecules. Especially, tunneling spectroscopy (TS) can probe current-voltage behavior, which depends on electronic state of individual molecules. It has been reported that a single organic molecule on a metal surface was successfully identified [8], and chemically inequivalent molecules with nearly identical geometric structure and size were distinguished by tunneling spectroscopy measurements [9].

Recently, a distinctive current-voltage behavior called negative differential resistance (NDR) phenomenon has garnered great attention as a probe of electronic state of molecule in tunneling spectroscopy of semiconducting or insulating materials [10,11]. The NDR phenomenon is explained by a few models [12,13], but mostly resonant tunneling through a double-barrier quantum well structure [14]; when the incident electron matches with a virtual empty state in the molecular well, tunneling current can pass without attenuation through the molecular well. Therefore, the electronic state of the molecule can be estimated from NDR phenomenon. It has been reported that Keggin heteropolyacids (HPAs) also exhibited NDR phenomenon [15,16].

HPAs are early transition metal-oxygen anion clusters that have been widely employed as catalysts for various homogeneous and heterogeneous reactions in acid and oxidation catalysis [17]. HPAs exhibit a wide range of molecular sizes, compositions, and molecular architectures. Among various structural classes, Keggin HPAs have been widely employed as acid and oxidation catalysts in commercial processes [18,19]. Recently, however, Wells-Dawson HPAs have also attracted much attention as promising catalysts due to their excellent catalytic activity for several oxidation reactions [20]. Because of the importance of comprehensive investigation about catalytic redox properties of HPAs in designing oxidation catalysts, several previous researches attempted to elucidate redox properties of HPAs by quantum chemical molecular orbital study [21], electrochemical measurement [22], and UV-visible spectroscopy [23]. However, not much progress has been made on the redox properties of Wells-Dawson HPAs, and only limited information is available in the literature.

In this work, STM and tunneling spectroscopy studies of niobium-containing $H_{6+x}P_2W_{18-x}Nb_xO_{62}$ (x=0, 1, 2, 3) Wells-Dawson HPAs were carried out to examine their redox properties. To find out possibility of STM as a promising technique to probe redox property of the HPAs, NDR peak voltage was correlated with reduction potential and absorption edge energy determined by electrochemical method and UV-visible spectroscopy, respectively. Vapor-phase oxidative dehydrogenation of isobutyraldehyde to methacrolein was carried out as a model reaction to probe oxidation catalysis of the HPAs. A correlation between NDR peak voltage and oxidation catal-

†To whom correspondence should be addressed.
E-mail: inksong@snu.ac.kr

ysis of the HPAs was then established.

EXPERIMENTAL

1. Catalyst

Niobium-containing $H_{6+x}P_2W_{18-x}Nb_xO_{62}$ (x=0, 1, 2, 3) Wells-Dawson HPAs were prepared via $Na_{12}P_2W_{15}O_{56}$ lacunary HPA according to the method in our previous work [24] using $Na_2WO_4 \cdot 2H_2O$ (Junsei Chem.), phosphoric acid (Sigma-Aldrich), acetic acid (Samchun Chem.), $NbCl_5$ (Sigma-Aldrich), oxalic acid (Sigma-Aldrich), KCl (Junsei Chem.), diethyl ether (Samchun Chem.), and HCl (Sigma-Aldrich). Successful formation of niobium-containing $H_{6+x}P_2W_{18-x}Nb_xO_{62}$ (x=0, 1, 2, 3) Wells-Dawson HPAs was confirmed by FT-IR (Nicolet, Nicolet 6700), ^{31}P-NMR (Bruker, AVANCE 600), and ICP-AES (Shimadzu, ICPS-1000IV) analyses, as reported in a previous work [24]. In this work, $H_{6+x}P_2W_{18-x}Nb_xO_{62}$ Wells-Dawson HPAs with x=0, 1, 2, and 3 were denoted as WD-Nb_0, WD-Nb_1, WD-Nb_2, and WD-Nb_3, respectively.

2. Scanning Tunneling Microscopy and Tunneling Spectroscopy

0.01 M of aqueous solutions of $H_{6+x}P_2W_{18-x}Nb_xO_{62}$ (x=0, 1, 2, 3) Wells-Dawson HPAs were prepared. Small amount of each sample solution was deposited on highly oriented pyrolytic graphite (HOPG) and dried in atmosphere for approximately 1 h. HPA was physically deposited on graphite surface, and any other chemical interaction between HPA and graphite surface did not exist. STM and TS investigations of deposited samples were carried out using an Autoprobe CP instrument (thermomicroscope) in atmosphere. Mechanically formed Pt/Ir (90/10) tips were used as probes. STM tips were first calibrated by imaging bare HOPG and by confirming its standard periodicity (2.46 Å). Scanning was done in the constant current mode at a tunneling current of 1-2 nA and a sample bias of +100 mV. The image presented in this work was not filtered. The lattice constant of unit cell was determined from 2-dimensional fast Fourier transform (2D FFT) analyses. To measure tunneling spectra of the HPAs, the STM probe was positioned above the HPA molecule of interest and tunneling current was monitored while bias voltage was ramped from −2 to +2 V with respect to the tip. The voltage axis in the tunneling spectrum represents the potential applied to the sample relative to that of the tip. Current-voltage spectra were measured several times with three different tips in order to get more accurate and reproducible results and to provide a basis for statistical analyses.

3. Oxidative Dehydrogenation of Isobutyraldehyde to Methacrolein

Vapor-phase oxidative dehydrogenation of isobutyraldehyde to methacrolein was carried out as a model reaction to probe oxidation catalysis of niobium-containing $H_{6+x}P_2W_{18-x}Nb_xO_{62}$ (x=0, 1, 2, 3) Wells-Dawson HPAs. Reaction was performed under atmospheric pressure in a fixed-bed reactor. 0.5 g of HPA catalyst was charged into a tubular pyrex reactor and pretreated with a mixed stream of nitrogen (10 ml/min) and oxygen (10 ml/min) at 280 °C for 1 h. Isobutyraldehyde (0.15 ml/h) was sufficiently vaporized by passing through a preheating zone and was continuously fed into the reactor together with nitrogen (10 ml/min) and oxygen (10 ml/min). Catalytic reaction was carried out at 270 °C for 5 h. Reaction products were periodically sampled and analyzed by gas chromatography (HP 5890, FID) equipped with a capillary column (Supelco, VO COL, 60 m×1.5 μm×0.25 mm). Conversion of isobutyraldehyde, selectivity for methacrolein, and yield for methacrolein were calculated on the basis of carbon balance.

RESULTS AND DISCUSSION

1. Scanning Tunneling Microscopy of $H_{6+x}P_2W_{18-x}Nb_xO_{62}$ Wells-Dawson HPAs

Fig. 1 shows the molecular structure of Wells-Dawson heteropolyanion. Heteropolyanion is polymeric oxoanion that consists of central heteroatom (X), polyatom (M), and oxygen. Molecular structure of Wells-Dawson heteropolyanion, $[X_2M_{18}O_{62}]^{m-}$, consists of two defect Keggin-type fragments, $[XM_9O_{34}]^{n-}$. Each fragment consists of a central tetrahedron (XO_4) surrounded by nine octahedrons (MO_6), and three octahedral sites remain as a defect site. The nine octahe-

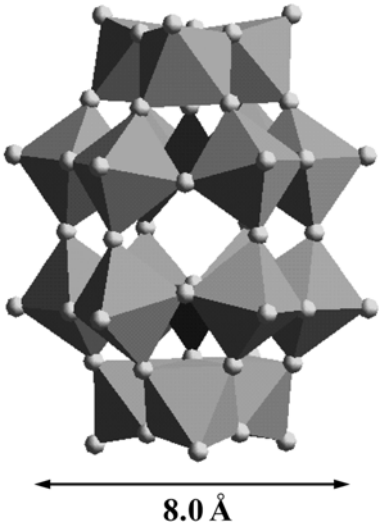

Fig. 1. Molecular structure of Wells-Dawson heteropolyanion.

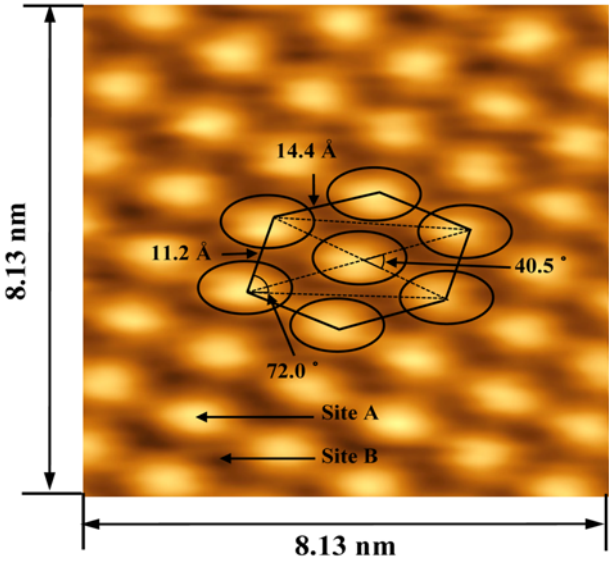

Fig. 2. STM image $H_6P_2W_{18}O_{62}$ Wells-Dawson HPA deposited on graphite.

drons comprise three groups of three edge-shared units (M_3O_{13}), which have an oxygen connected to central heteroatom. Two defect Keggin-type units are linked through six metal-oxygen-metal bonds and form a rugby ball-shaped Wells-Dawson heteropolyanion. Because various metals or semimetals or even non-metals can be incorporated into the molecular structure of heteropolyanion as heteroatom and polyatom, catalytic properties of the HPAs are easily tuned by changing the identity of heteroatom and framework polyatom. In Fig. 1, niobium of $H_{6+x}P_2W_{18-x}Nb_xO_{62}$ (x=0, 1, 2, 3) Wells-Dawson HPAs is incorporated on the "cap" site of the Wells-Dawson structure one by one.

Fig. 2 shows the STM image of $H_6P_2W_{18}O_{62}$ Wells-Dawson HPA deposited on graphite. The STM image clearly shows the formation of self-assembled and well-ordered array of heteropolyanions on graphite surface. Each bright site (denoted as Site A in Fig. 2) corresponded to individual heteropolyanion molecules. The periodicity of the unit cell constructed on the basis of lattice constants determined from two-dimensional fast Fourier transform (2D FFT) is 11.2×14.4 Å. The measured lattice constants of $H_6P_2W_{18}O_{62}$ array are in good agreement with the lattice constants of Wells-Dawson HPA determined by X-ray crystallography [25].

2. Tunneling Spectroscopy of $H_{6+x}P_2W_{18-x}Nb_xO_{62}$ Wells-Dawson HPAs

Fig. 3 shows the typical tunneling spectra of $H_6P_2W_{18}O_{62}$ Wells-Dawson HPA taken at two different sites, denoted as Site A and B in Fig. 2. Tunneling spectrum taken at Site B was identical to that of bare graphite surface, indicating that the two-dimensional array of HPA shown in Fig. 2 is monolayer. However, tunneling spectrum taken at Site A in Fig. 2 shows a distinctive current-voltage behavior referred to as NDR, showing an NDR peak in the range of negative bias voltage. In this work, NDR peak voltage is defined as the voltage where the maximum tunneling current is observed in this distinctive current-voltage region.

Fig. 4 shows the distribution of NDR peak voltages of $H_6P_2W_{18}O_{62}$ Wells-Dawson HPA. The NDR measurements were carried out several times atop the bright corrugations in order to obtain more accurate and reproducible results and to provide a basis of statistical analyses. For $H_6P_2W_{18}O_{62}$ Wells-Dawson HPA, the statistical average value of NDR peak voltages was found to be −1.13±0.07 V. In this work, the average NDR peak voltage was taken as the representative NDR peak voltage of the HPA. NDR peak voltages of $H_{6+x}P_2W_{18-x}Nb_xO_{62}$ (x=0, 1, 2, 3) Wells-Dawson HPAs are summarized in Table 1.

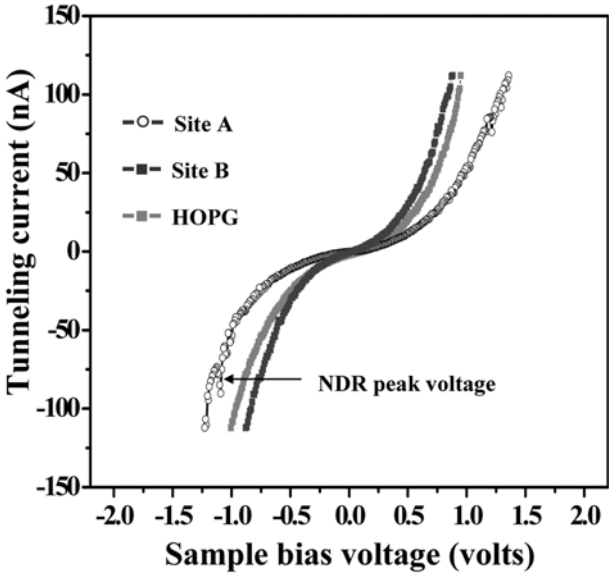

Fig. 3. Typical tunneling spectra of $H_6P_2W_{18}O_{62}$ Wells-Dawson HPA taken at two different sites, denoted as Site A and B in Fig. 2.

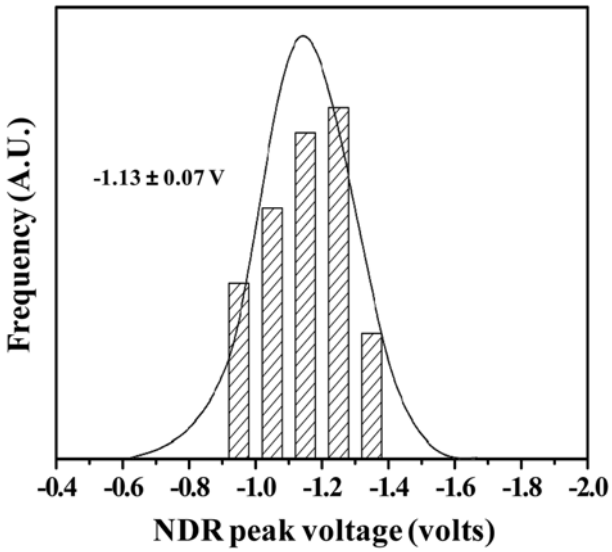

Fig. 4. Distribution of NDR peak voltages of $H_6P_2W_{18}O_{62}$ Wells-Dawson HPA.

Table 1. NDR peak voltages, Reduction potentials, and absorption edge energies of $H_{6+x}P_2W_{18-x}Nb_xO_{62}$ (x=0, 1, 2, 3) Wells-Dawson HPAs determined by tunneling spectroscopy, electrochemical method, and UV-visible spectroscopy, respectively

Catalyst	NDR peak voltage (volts)	Reduction potential (SCE, volts)[a]	Absorption edge energy (eV)[a]
WD-Nb_3	−1.08±0.09	−0.560	3.73
WD-Nb_2	−1.06±0.10	−0.555	3.71
WD-Nb_1	−1.02±0.09	−0.539	3.67
WD-Nb_0	−1.13±0.07	−0.576	3.77

[a]Data were taken from a literature [24]

3. Correlations of NDR Peak Voltage of $H_{6+x}P_2W_{18-x}Nb_xO_{62}$ Wells-Dawson HPAs with Reduction Potential and Absorption Edge Energy

A quantum chemical molecular orbital study of the HPAs reveals that energy gap between the highest occupied molecular orbital (HOMO) and lowest unoccupied molecular orbital (LUMO) is well correlated with the reduction potential [21]. It is known that energy required for electron transfer from the HOMO to the LUMO can be measured by absorption edge energy determined by UV-visible spectroscopy [26]. Therefore, smaller UV-visible absorption edge energy corresponded to smaller energy gap between the HOMO and LUMO. An HPA with smaller energy gap is more reducible. In previous works [24,27], it was revealed that absorption edge energy of the HPAs showed the same trend as the trend of reduction poten-

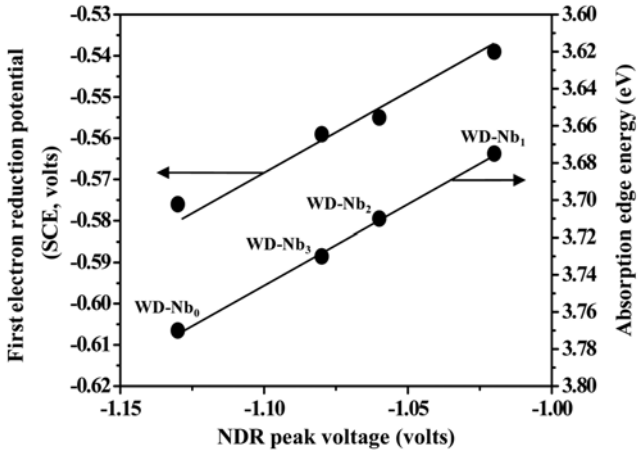

Fig. 5. Correlations of NDR peak voltage of $H_{6+x}P_2W_{18-x}Nb_xO_{62}$ (x= 0, 1, 2, 3) Wells-Dawson HPAs with reduction potential and absorption edge energy. Reduction potential and absorption energy were taken literature from the literature [24].

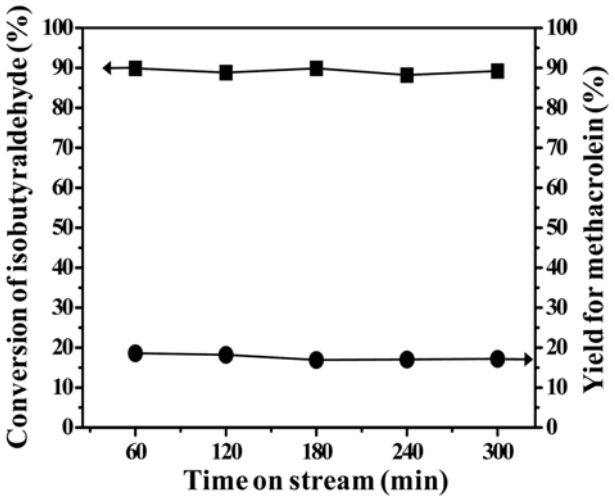

Fig. 6. Typical catalytic performance of $H_6P_2W_{18}O_{62}$ Wells-Dawson HPA in the vapor-phase oxidative dehydrogenation of isobutyraldehyde with time on stream at 270 °C.

tial, indicating that absorption edge energy could be utilized as a correlating parameter for redox property (reduction potential) of the HPA. Reduction potentials and absorption edge energies of $H_{6+x}P_2W_{18-x}Nb_xO_{62}$ (x=0, 1, 2, 3) Wells-Dawson HPAs which were taken from the literature [24] are summarized in Table 1.

Fig. 5 shows the correlations of NDR peak voltage of $H_{6+x}P_2W_{18-x}Nb_xO_{62}$ (x=0, 1, 2, 3) Wells-Dawson HPAs with reduction potential and absorption edge energy. It is noteworthy that the NDR peak voltage of $H_{6+x}P_2W_{18-x}Nb_xO_{62}$ Wells-Dawson HPAs appeared at less negative voltage with increasing reduction potential and with decreasing absorption edge energy. It has been reported that the HOMO of HPA is mostly composed of 2p-orbitals on the bridging oxygens of the HPAs, while the LUMO is a mixture of d-orbitals on the framework metal center and 2p-orbitals on the neighboring bridging oxygens [21]. Substitution of polyatom into HPA framework does not affect the energies of the HOMO which is entirely centered on the oxygens, while it does affect the LUMO, which is combination of 2p-orbitals in the bridging oxygens and d-orbital of the metals. Therefore, the energy gap of the HPA mostly depends on the energy state of the LUMO not the HOMO of the HPA. It can be inferred that less negative NDR voltage of the HPAs corresponds to lower energy state of the LUMO. Consequently, less negative NDR peak voltage value represents smaller energy gap between the HOMO and the LUMO, and in turn, higher reduction potential (more reducible) and lower absorption edge energy. Fig. 5 clearly shows that NDR peak voltage of $H_{6+x}P_2W_{18-x}Nb_xO_{62}$ Wells-Dawson HPAs determined by tunneling spectroscopy can serve as a correlating parameter for reduction potential and absorption edge energy of the HPAs.

4. Oxidative Dehydrogenation of Isobutyraldehyde to Methacrolein over $H_{6+x}P_2W_{18-x}Nb_xO_{62}$ Wells-Dawson HPAs

In this work, oxidative dehydrogenation of isobutyraldehyde to methacrolein was carried out as a model reaction to probe oxidation catalysis of niobium-containing $H_{6+x}P_2W_{18-x}Nb_xO_{62}$ Wells-Dawson HPA catalysts. It is known that methacrolein was mainly produced through oxidative dehydrogenation of isobutyraldehyde by consuming lattice oxygen of HPA [28,29]. In our catalytic reaction, acetone, water, CO, and CO_2 were produced as by-products.

Fig. 6 shows the typical catalytic performance of $H_6P_2W_{18}O_{62}$ Wells-Dawson HPA in the vapor-phase oxidative dehydrogenation of isobutyraldehyde with time on stream at 270 °C. $H_6P_2W_{18}O_{62}$ Wells-Dawson HPA showed a stable catalytic performance. Conversion of isobutyraldehyde and yield for methacrolein over $H_6P_2W_{18}O_{62}$ Wells-Dawson HPA were almost constant with time on stream. Other niobium-containing HPAs also showed a stable performance with time on stream. Yield for methacrolein obtained after a 5 h-reaction increased in the order of WD-Nb_0 (17.2%)<WD-Nb_3 (19.1%)<WD-Nb_2 (19.8%)<WD-Nb_1 (21.6%).

Fig. 7 shows the correlation between NDR peak voltage of $H_{6+x}P_2W_{18-x}Nb_xO_{62}$ (x=0, 1, 2, 3) Wells-Dawson HPAs and yield for methacrolein. The correlation clearly shows that the NDR peak voltage of $H_6P_2W_{18}O_{62}$ Wells-Dawson HPAs appeared at less negative applied voltage with increasing yield for methacrolein. This demonstrates that NDR peak voltage of $H_{6+x}P_2W_{18-x}Nb_xO_{62}$ (x=0, 1, 2, 3) Wells-Dawson HPAs can also be utilized as a correlating parameter for

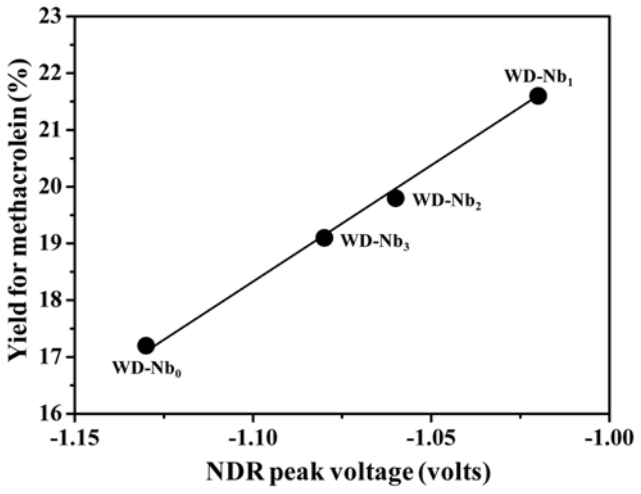

Fig. 7. Correlation between NDR peak voltage of $H_{6+x}P_2W_{18-x}Nb_xO_{62}$ (x=0, 1, 2, 3) Wells-Dawson HPAs and yield for methacrolein.

oxidation catalysis of the HPAs.

CONCLUSIONS

Scanning tunneling microscopy and tunneling spectroscopy studies of niobium-containing $H_{6+x}P_2W_{18-x}Nb_xO_{62}$ (x=0, 1, 2, 3) Wells-Dawson HPAs were carried out to elucidate their redox properties. STM image clearly showed the formation of self-assembled and well-ordered array of heteropolyanions on graphite surface. In tunneling spectroscopy measurements, $H_{6+x}P_2W_{18-x}Nb_xO_{62}$ Wells-Dawson HPAs exhibited a distinctive current-voltage behavior referred to as NDR. In order to correlate NDR peak voltage of the HPAs with redox property, reduction potential and absorption edge energy determined by electrochemical method and UV-visible spectroscopy, respectively, were compared. It was revealed that NDR peak voltage of the HPAs appeared at less negative voltage with increasing reduction potential and with decreasing absorption edge energy. Vapor-phase oxidative dehydrogenation of isobutyraldehyde to methacrolein was carried out as a model reaction to probe oxidation catalysis of $H_{6+x}P_2W_{18-x}Nb_xO_{62}$ Wells-Dawson HPAs. Correlation between NDR peak voltage of the HPAs and yield for methacrolein clearly showed that NDR peak voltage of the HPAs appeared at less negative voltage with increasing yield for methacrolein. In conclusion, NDR peak voltage of niobium-containing $H_{6+x}P_2W_{18-x}Nb_xO_{62}$ (x=0, 1, 2, 3) Wells-Dawson HPAs could be utilized as a correlating parameter for redox property (reduction potential and absorption edge energy) and as a probe of oxidation catalysis in the oxidative dehydrogenation of isobutyraldehyde.

ACKNOWLEDGEMENTS

This work was supported by Mid-career Researcher Program of National Research Foundation (NRF) grant funded by the Korea government (MEST) (No. 2010-0000301).

REFERENCES

1. J. V. Barth, G. Costantini and K. Kern, *Nature*, **437**, 671 (2005).
2. H. Tomimoto, R. Sumii, N. Shirota, N. Yagi, M. Taniguchi, T. Sekitani and K. Tanaka, *J. Vac. Sci. Technol. B*, **18**, 2335 (2000).
3. J. S. Prauzner-Bechcicki, S. Godlewski, A. Tekiel, P. Cyganik, J. Budzioch and M. Szymonski, *J. Phys. Chem. C*, **113**, 9309 (2009).
4. S. Suzuki, Y. Yamaguchi, H. Onishi, K. Fukui, T. Sasaki and Y. Iwasawa, *Catal. Lett.*, **50**, 117 (1998).
5. K. Takimoto, R. Kuroda, S. Shido, S. Yasuda, H. Matsuda, K. Eguchi and T. Nakagiri, *J. Vac. Sci. Technol. B*, **15**, 1429 (1997).
6. J. V. Lauritsen, R. T. Vang and F. Besenbacher, *Catal. Today*, **111**, 34 (2006).
7. J. Matthiesen, S. Wendt, J. Ø. Hansen, G. K. H. Madsen, E. Lira, P. Galliker, E. K. Vestergaard, R. Schaub, E. Laegsgaard, B. Hammer and F. Besenbacher, *ACS Nano*, **3**, 517 (2009).
8. B. C. Stipe, M. A. Rezaei and W. Ho, *Science*, **280**, 1732 (1998).
9. M. K.-J. Johansson, S. M. Gray and L. S. O. Johansson, *J. Vac. Sci. Technol. B*, **14**, 1015 (1998).
10. H.-J. Müssig, D. Krüger, S. Hinrich and P. O. Hansson, *Surf. Sci.*, **314**, L884 (1994).
11. N. P. Guisinger, M. E. Greene, R. Basu, A. S. Baluch and M. C. Hersam, *Nano Lett.*, **4**, 55 (2004).
12. M. Grobis, A. Wachowiak, R. Yamachika and M. F. Crommie, *Appl. Phys. Lett.*, **86**, 204102 (2005).
13. Z. Fan, K. Chen, Q. Wan, B. S. Zou, W. Duan and Z. Shuai, *Appl. Phys. Lett.*, **92**, 263304 (2008).
14. S. M. Lindsay, O. F. Sankey, Y. Li and C. Herbst, *J. Phys. Chem.*, **94**, 4655 (1990).
15. I. K. Song, M. S. Kaba, G. Coulston, K. Kourtakis and M. A. Barteau, *Chem. Mater.*, **8**, 2352 (1996).
16. I. K. Song and M. A. Barteau, *Korean J. Chem. Eng.*, **19**, 567 (2002).
17. N. Mizuno and M. Misono, *Chem. Rev.*, **98**, 199 (1998).
18. D. R. Park, U. G. Hong, S. H. Song, J. G. Seo, S.-H. Baeck, J. S. Chung and I. K. Song, *Korean J. Chem. Eng.*, **27**, 465 (2010).
19. Y. Bang, D. R. Park, Y. J. Lee, J. C. Jung and I. K. Song, *Korean J. Chem. Eng.*, **27**, 79 (2011).
20. L. E. Briand, G. T. Baronetti and H. J. Thomas, *Appl. Catal. A: Gen.*, **256**, 37 (2003).
21. R. S. Weber, *J. Phys. Chem.*, **98**, 2999 (1994).
22. F. Jonnevijlle, C. M. Tourné and G. F. Tourné, *Inorg. Chem.*, **21**, 2742 (1982).
23. D. R. Park, J. H. Song, S. H. Lee, S. H. Song, H. Kim, J. C. Jung and I. K. Song, *Appl. Catal. A: Gen.*, **349**, 222 (2008).
24. D. R. Park, J. H. Choi, S. Park and I. K. Song, *Appl. Catal. A: Gen.*, **394**, 201 (2011).
25. B. Dawson, *Acta. Cryst.*, **6**, 113 (1953).
26. T. Yamase, *Chem. Rev.*, **98**, 307 (1998).
27. M. H. Youn, D. R. Park, J. C. Jung, H. Kim, M. A. Barteau and I. K. Song, *Korean J. Chem. Eng.*, **24**, 51 (2007).
28. J. Hu, R. C. Burns and J. Guerbois, *J. Mol. Catal. A: Chem.*, **152**, 141 (2000).
29. M. Misono, *Polyoxometalates: From platonic solid to anti-retroviral activity*, Kluwer, Dordrecht (1994).